Host-directed therapy for intracellular bacterial Infections

Korbee, C.J.

4 | Novel Host-Directed Chemical Compounds Inhibit Intracellular Bacteria by Targeting PCTAIRE Kinases

Cornelis J. Korbee*, Matthias T. Heemskerk*, Kimberley V. Walburg, Rian van den Nieuwendijk, Elisabeth van Strijen, Coenraad Kuijl, Conrad Schreuders, Janneke Eken, Nigel D.L Savage, Jacques J. Neefjes, Hermen S. Overkleeft, Tom H. M. Ottenhoff**, Mariëlle C. Haks**

Rapidly increasing drug-resistance poses severe problems in combatting many bacterial infectious diseases, including tuberculosis (TB) and *Salmonella* infections. Recent attempts to identify novel antibiotics have yielded only limited numbers of leads, prompting for novel approaches, including host-directed therapies. Intracellular pathogens like *Mycobacterium tuberculosis* (*Mtb*) and *Salmonellae* manipulate host signaling networks to promote their survival, but very few host targets and chemical compounds have been identified for host-directed therapies. Using a chemical genetic approach focused on a novel, proprietary library of chemical compounds derived from the host-directed inhibitor of intracellular bacteria H-89, we here identify novel kinase inhibitor 97i as a host-directed inhibitor of intracellular *Mtb* and *Salmonella* typhimurium (*Stm*). 97i Strongly inhibited both (MDR-)*Mtb* and *Stm* infection in human (phagocytic) cell lines and in primary Mϕ1 and Mϕ2 macrophages. Importantly, we identify the PCTAIRE-family kinase CDK18 as a novel host factor controlling intracellular *Stm*, and as a direct target of 97i. Together, these results identify PCTAIRE kinases as novel putative target molecules for host-directed therapies (HDT) and 97i as a strong basis for HDT drug development for intracellular bacterial infections.

Manuscript in preparation

* Contributed equally
** Contributed equally

Introduction

Tuberculosis (TB) remains a critical global health problem with an estimated one fourth of the world population carrying a latent *Mycobacterium tuberculosis* (*Mtb*) infection and 10.4 million new cases and 1.8 million deaths annually[1,2]. The emergence of multi-, extensively- and totally drug-resistant (MDR/XDR/TDR) strains of *Mtb* further aggravates this situation, threatening to render current antibiotics inadequate for future TB treatment[3-5]. An estimated 490,000 people were diagnosed with MDR-TB in 2016[2].

Salmonella enterica infections are major causes of morbidity and mortality worldwide as well, particularly *S. enterica* serovar Typhi (the causative agent of typhoid fever), which causes between 128,000 and 161,000 deaths annually (World Health Organization figures January 2018; http://www.who.int/news-room/fact-sheets/detail/typhoid). As with TB, antibiotic resistance is becoming an increasing problem for treatment of typhoid fever, prompting for novel approaches[6].

Several novel candidate antibiotics have recently been identified[7], but because current antibiotics already cover the majority of drugable targets of pathogens, it is increasingly difficult to discover new classes of antibiotics[8-14]. However, new drugs are urgently needed to combat the rapidly increasing global drug resistance for many human pathogens. Intracellular bacteria such as *Salmonellae* and *Mtb* present additional challenges to treatment and eradication by host defense mechanisms, as they are able to manipulate host-signaling networks to inhibit phagosome maturation, apoptosis, autophagy and MHC restricted antigen presentation to T cells, thereby subverting both innate and adaptive immunity. Better knowledge of the mechanisms that these and other intracellular pathogens deploy to escape host defense is critical to discover opportunities for novel therapies, including treatment strategies that target host rather than pathogen molecules (host-directed therapy; HDT). Importantly, chemical-genetic and pharmacological reprogramming of host immune functions may not only be effective against drug-resistant bacteria, but also help to restore host control of infected cells that are metabolically perturbed[15,16]. The feasibility of such HDT approaches to improve bacterial inhibition both *in vitro* in human cells and *in vivo* in mouse, rabbit and zebrafish models has recently been shown in several studies, including our own[17-34].

In one of the first studies in this area, we used reciprocal chemical-genetics focusing on systematic perturbation of the human kinome and identified AKT1 as a central molecule regulating intracellular survival of *Salmonella enterica* serovar Typhimurium *(Stm)* and *Mtb*, including MDR-*Mtb*[17]. We demonstrated that by targeting AKT1 the kinase inhibitor H-89 significantly decreased intracellular bacterial loads in human cell lines and in primary macrophages. However, compared to treatment of *Stm*-infected cells, inhibition of intracellular *Mtb* by H-89 was less efficient, suggesting that *Mtb* also modulates other host signaling pathways to subvert its intracellular killing that are not affected by H-89. Indeed, *Mtb* has been reported to arrest vesicle maturation at an earlier stage than *Stm*[17,35,36], such that other regulators of phagosome maturation, including kinases, may need to be targeted. In agreement with this notion, Kumar *et al*.

demonstrated that silencing of AKT1 alone was not sufficient to induce efficient killing of *Mtb*, and found that the combined knock-down of AKT1 and AKT2 resulted in a significant decrease in bacterial outgrowth[18]. Collectively, these studies suggest that in addition to AKT1, the perturbation of other host targets or combinations of host targets will be essential to efficiently inhibit intracellular *Mtb* by HDT, but the precise molecular host targets remain largely unknown.

Other kinases that may be involved in host-mediated inhibition of *Mtb* include Imatinib-sensitive kinases like ABL1 and ABL2, and enhanced control of *Mtb* could be achieved in Imatinib-treated mice[22]. Our most recent work used chemical genetic experimental and computational approaches, and uncovered receptor and non-receptor tyrosine kinase (RTK) signaling as a novel important host pathway controlling intracellular *Mtb* survival. This pathway was drugable by compounds and drugs currently in clinical trials for other diseases including Dovitinib, AT9283 and ENMD-2076, thus offering new approaches to combat TB in the face of rapidly rising multi-drug resistance[34]. In particular, inhibitors of growth factor receptor tyrosine kinases were identified in this study, corroborating other studies linking growth factor receptors like epidermal growth factor receptor (EGFR) and vascular endothelial growth factor receptor (VEGFR) and corresponding inhibitors like gefitinib and pazopanib to *Mtb* infection outcome[29,32,37].

In addition to kinases and kinase inhibitors, several other potential targets and compounds for HDT for TB were recently identified, ranging from immunomodulatory drugs to metabolic targets. Sundaramurthy *et al*. identified two antipsychotics (Haloperidol and Prochlorperazine) and an antidepressant (Nortryptiline) that displayed host-directed mycobacterial inhibition by enhancing phagocytic and autophagic macrophage responses[20]. Machado *et al*. identified the ion channel blockers Verapamil, Thioridazine, Chlorpromazine, Flupenthixol and Haloperidol as *Mtb*-inhibiting compounds that enhance efficacy of antibiotics by inhibiting efflux activity in the bacterium. Interestingly, these compounds also displayed host-mediated bacterial inhibition by enhancing phagosome acidification and upregulating lysosomal hydrolase activity[21]. Singhal *et al.* reported the anti-diabetic drug Metformin as a host-directed compound that inhibited *Mtb* by increasing production of mitochondrial reactive oxygen species and promoting phagosome-lysosome fusion[38].

Another challenge in TB therapy that may be overcome by HDT strategies is the limited antibiotics efficacy and their limited penetration in granulomas[28]. Similar to tumor treatment strategies, antiangiogenic treatment may decrease hypoxic fractions of granulomas and enhance drug penetration. Using anti-VEGF antibodies or inhibitors of the VEGF pathway were demonstrated to be a promising strategy to achieve this *in vitro* and in rabbit and zebrafish models[28,29,34]. In another report, Simvastatin was identified as a drug repurposing candidate for TB[31]. The authors reported that Simvastatin treatment both *in vitro* and *in vivo* greatly enhanced isoniazid efficacy, possibly by limiting access of *Mtb* to intracellular nutrient-rich lipid droplets.

Despite all these recent advances, HDT drug development for intracellular bacterial infections has not yet led to clinically applicable and efficacious drug regimens. A better understanding of the host-pathogen interactions and in

particular the molecular host targets which are critical to controlling intracellular infection is needed to rationally design or repurpose drugs that can be applied clinically.

In the current study we have explored the kinase inhibitor chemical space, using different chemical and functional infection biology approaches, and identified novel chemical compounds that are active in controlling intracellular bacterial infection. Structure-activity analysis of the compound library revealed a correlation between compounds' structural features and their ability to inhibit AKT1, which directly corresponded to their ability to inhibit intracellular *Stm*. However, no such correlation was observed when assessing the compounds' ability to inhibit intracellular *Mtb*, suggesting involvement of kinases other than AKT1 in host regulation of intracellular *Mtb*. Perhaps most importantly, the host-mediated antimicrobial activity induced by kinase inhibitor 97i greatly exceeded that of currently known HDT drug candidates. Finally, we demonstrate that the PCTAIRE kinase CDK18 is a target of 97i that is central to host control of intracellular *Stm* and possibly (MDR-)*Mtb.*

Results

H-89 treatment and AKT1 silencing efficiently decrease intracellular *Stm* bacterial loads but are less efficient against intracellular *Mtb*.

We previously identified AKT1 as a central regulator of *Stm* intracellular survival in primary human macrophages and the AKT1 inhibitor H-89 as a novel host-directed inhibitor of *Stm* and *Mtb*[17]. More recently we reported the development of a fast and versatile flow cytometry-based assay to allow for medium-throughput screening of chemical and genetic libraries in cell lines infected with *Stm* or *Mtb*[34]. As important validation data we first verified the bacterial inhibition resulting from AKT1 silencing and H-89 treatment in this new model, using *Stm* and *Mtb* human (phagocytic) cell line based infection models. Indeed, both H-89 treatment and AKT1 silencing significantly reduced the bacterial load in HeLa cells infected with *Stm* and in MelJuSo cells infected with *Mtb* H37Rv, lending important validation of our previous findings in macrophages as well as providing key validation of the model for further application in chemical genetic screens (**Figure 1**).

As previously also reported, the extent of the effect of H-89 treatment and AKT1 silencing was much less pronounced for *Mtb* than for *Stm* (**Figure 1**), indicating that host kinases other than those targeted by H-89 may be important in regulating *Mtb* intracellular survival. To identify these, we explored the kinase inhibitor chemical space by following a chemical genetic screening approach using a newly synthesized chemical compound library based on the H-89 backbone.

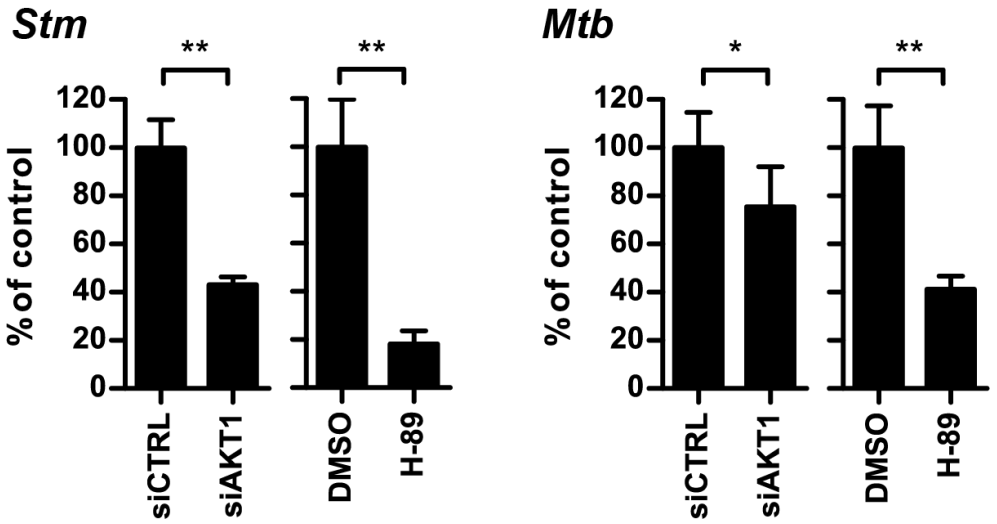

⬆ Figure 1. Inhibition or silencing of AKT1 decreases *Stm* and *Mtb* bacterial load.
AKT1 silencing by siRNA or treatment with 10 μM H-89 or DMSO at equal v/v in HeLa cells infected with *Stm* (left panel) or MelJuSo cells infected with *Mtb* (right panel). Bacterial load was determined by flow cytometry and is displayed as percentage of the appropriate negative control (DMSO for compounds and siCTRL for siRNA, respectively). Bars display mean ± standard deviation of 6 technical replicates. A representative result out of at least 10 experiments is shown. Statistical significance was tested using a t-test.
(* = p-value <0.05, ** = p-value <0.01).

Identification of novel kinase inhibitors with enhanced activity against *Mtb* and *Stm*.

We synthesized a novel library of 76 H-89-analogue compounds by systematically altering residues on 3 key positions at the styrene moiety of the chemical backbone of H-89 (**Figure 2**; synthesis described in "Synthetic studies on kinase inhibitors and cyclic peptides: strategies towards new antibiotics", Adriaan W. Tuin, 2008) and screened this library using our novel flow cytometry-based assay[34]. Using this assay, a population of *Stm*-infected cells with high fluorescence intensity (*Stm* 'bright') can be discerned, which is indicative of cells harboring proliferating bacteria. This population was found to be sensitive to H-89 treatment. In contrast, H-89 treatment did not affect the total fraction of *Stm*-infected cells (*Stm* total). Screening of the compound library yielded 5 compounds that reduced the *Stm* bacterial load (z-score ≤ -2) and no compounds that enhanced bacterial survival when analyzing the *Stm* 'bright' population (**Figure 3A, top panel**; z-score ≥ 2). In contrast, the total *Stm* infected population was decreased by 2 compounds (97a and 97i), while 8 compounds increased *Stm* total (**Figure 3A, middle panel**). In the MelJuSo-*Mtb* model, 36 compounds

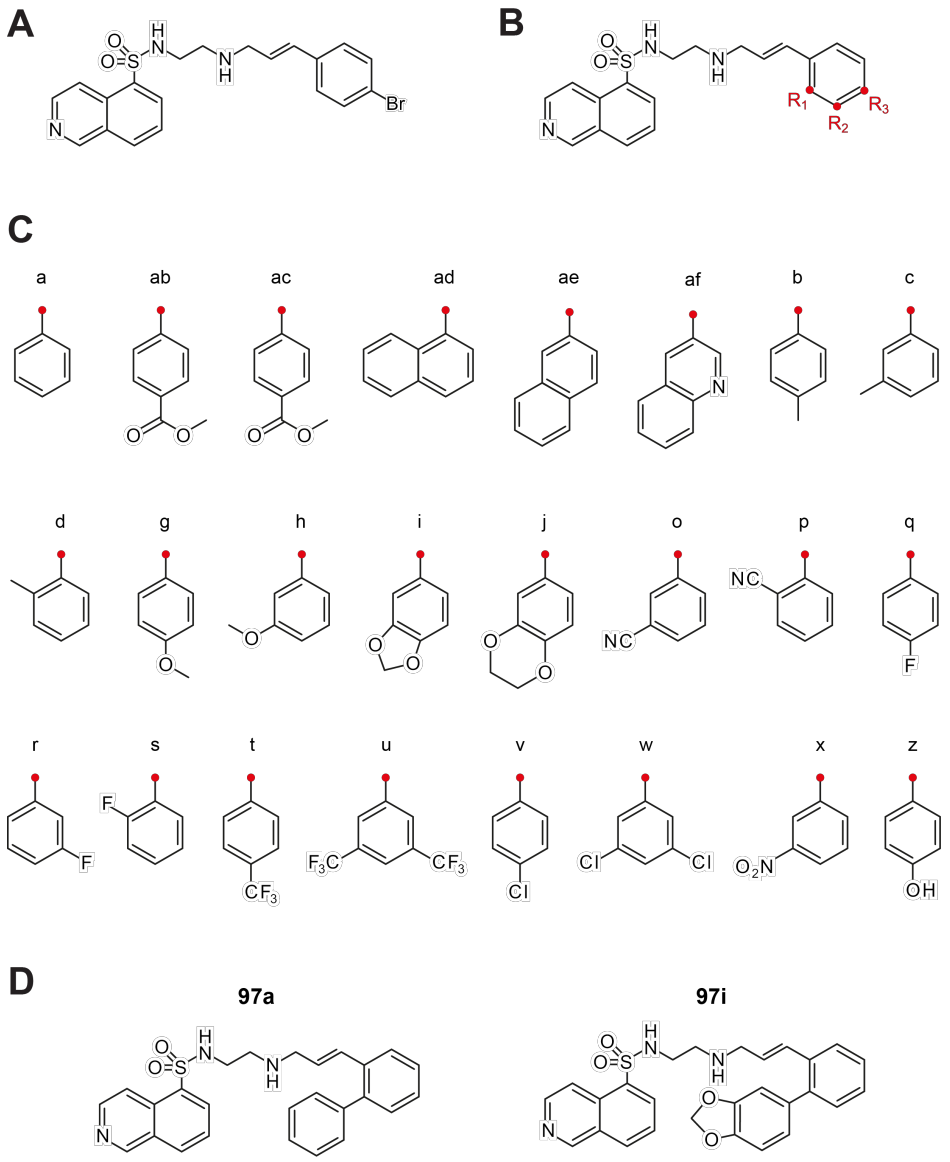

⬆ Figure 2. Construction of the H-89-based chemical library and structure of lead compounds.

A. Chemical structure of H-89. **B.** H-89-derived chemical backbone of the inhibitor library. Red nodes indicate the positions (R_1, R_2 and R_3) where chemical residues were attached to construct the library. **C.** Names and chemical structures of the residues attached to the chemical backbone on either the R_1, R_2 or R_3 positions. The red nodes correspond to the R_1, R_2 or R_3 positions on the chemical backbone depicted in **A**. **D.** Chemical structures of compounds 97a (left panel) and 97i (right panel).

significantly inhibited *Mtb* and none of the compounds increased the bacterial load (**Figure 3A, bottom panel**). The two compounds that reduced the *Stm* total population (97a and 97i) also displayed remarkably strong inhibition of intracellular *Mtb.* As a strong inhibitory effect was observed in *Stm*- as well as in *Mtb*-infected cells, 97a and 97i might induce an inhibitory mechanism that is common for both *Stm* and *Mtb* infection. Inhibition of intracellular *Stm* and *Mtb* by 97a and 97i was subsequently confirmed in a rescreen and the effect of both compounds on host cell viability was assessed by analyzing total cell counts (**Figure 3B**). As 97a strongly affected host cell viability (especially in the MelJuSo-*Mtb* model), 97i was selected as our top candidate compound. To exclude that 97i exerted bacterial inhibition by a direct bactericidal or bacteriostatic mechanism instead of acting on host targets, we treated bacteria with 97i in bulk bacterial culture in the absence of human cells. No effect of H-89, 97a and 97i was seen on *Mtb* or *Stm* growth at a 10 μM concentration, either at neutral pH or for *Stm* grown in acidic broth (**Figure 3C**). As expected, *Mtb* did not proliferate in acidic broth regardless of compound treatment (data not shown).

The applicability of 97i as a novel TB HDT-drug was further explored in cell-based assays. As host-directed compounds do not directly affect bacteria, targeting the host should be equally effective in both WT and drug-resistant bacterial strains. Therefore, we treated primary human pro-inflammatory Mϕ1s and anti-inflammatory Mϕ2s infected with drug sensitive *Mtb* H37Rv (used in the experiments above) or MDR *Mtb* (Dutch outbreak 2003-1128 and Beijing strain 16319, specified in **Table 1**) with 97i. This resulted in a similar decrease in the bacterial loads of both MDR and non-MDR *Mtb* strains (**Figure 4A**). Thus, 97i-mediated *Mtb* inhibition by human macrophages is independent of bacterial drug resistance, further emphasizing the potential of host-directed therapeutic approaches for TB treatment. As host-directed treatment and antibiotics by

➡ Figure 3. Chemical compound screen of H-89 analogues.
A. HeLa-*Stm* (top and middle panels) and MelJuSo-*Mtb* (bottom panel) model-based chemical compound primary screening results at 10 μM concentration sorted by z-score. The top panel shows z-scores based on the percentage of brightly fluorescent cells (*Stm* 'bright'), while z-scores based on the total *Stm*-infected population (*Stm* total) are shown in the middle panel. Data points display the mean z-score ± standard deviation of 3 replicates. A z-score of 2 or -2 was used as a cut-off value for hit selection (indicated by dashed lines). **B.** Rescreen of compounds 97a and 97i in the MelJuSo-*Mtb* and HeLa-*Stm* infection models performed as in **A**, expressed as a percentage of the DMSO control. 97a, 97i and H-89 were used at 10 μM and DMSO at equal v/v was included as a negative control. Data are the mean percentage of the DMSO control ± standard deviation of 3 replicates. Statistical significance was tested using a one-way ANOVA. **C.** *Stm* and *Mtb* growth in liquid culture during treatment with 10 μM 97i or DMSO at equal v/v at pH 7.0 and pH 4.5. Fifty μg/ml gentamicin and 20 μg/ml rifampicin are displayed as positive controls for *Stm* and *Mtb* growth inhibition, respectively.
(** = p-value <0.01, *** = p-value <0.001).

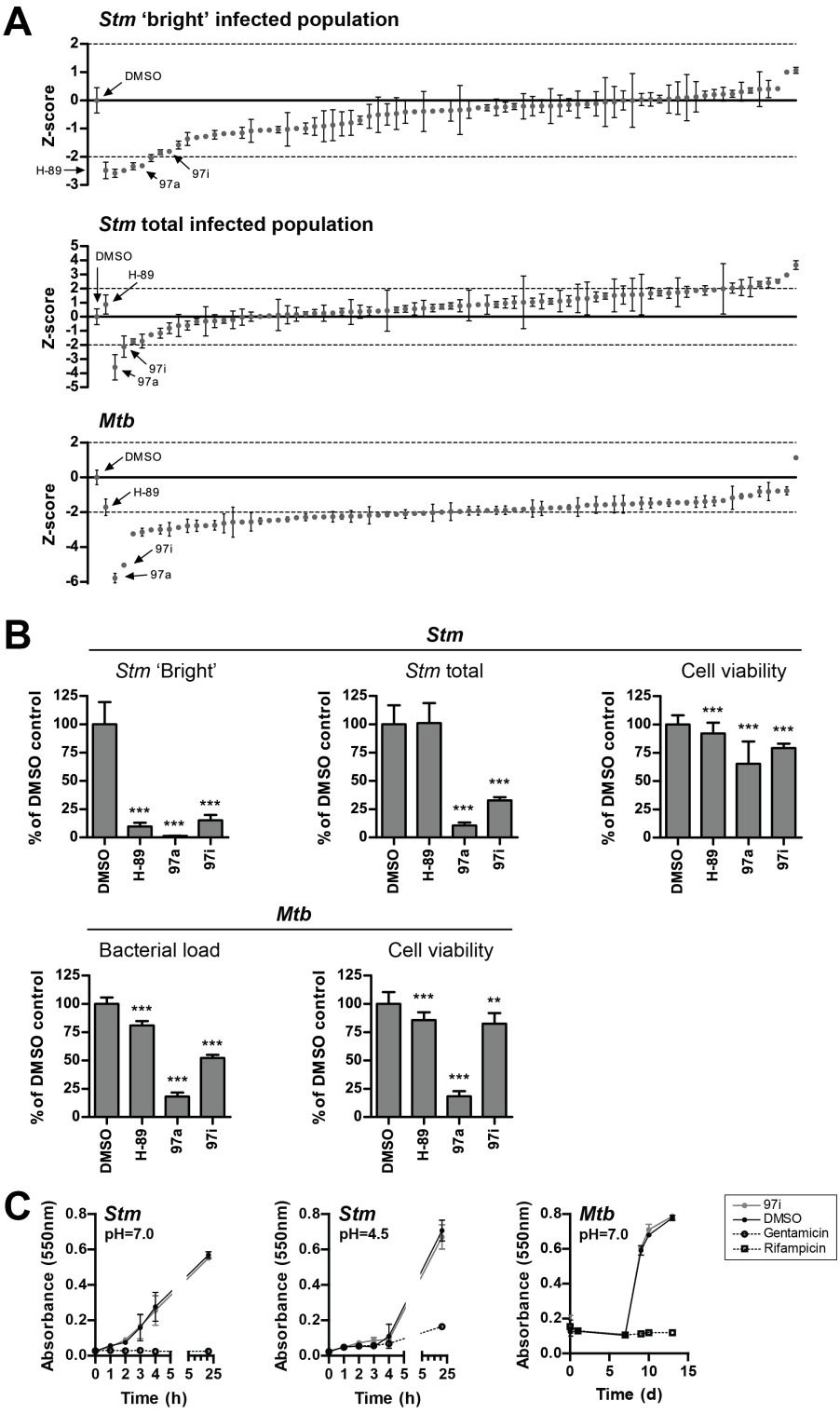
A
Stm 'bright' infected population
Z-score
DMSO
H-89
97a
97i
Stm total infected population
Mtb
B
Stm
Stm 'Bright'
Stm total
Cell viability
% of DMSO control
DMSO
H-89
97a
97i
Mtb
Bacterial load
Cell viability
C
Stm
pH=7.0
pH=4.5
Mtb
pH=7.0
Absorbance (550nm)
Time (h)
Time (d)
97i
DMSO
Gentamicin
Rifampicin

definition act on different pathways, we expected that treatment with host-targeting compounds might augment the effect of classical antibiotics. Indeed, treatment of MelJuSo cells infected with *Mtb* with a combination of rifampicin and 97i resulted in an additional decrease in bacterial survival as compared to rifampicin alone, both at optimal and suboptimal antibiotic concentrations (**Figure 4B**).

Thus, 97i is a novel H-89-analogue kinase inhibitor that strongly inhibits intracellular *Stm* and *Mtb* in a host-directed fashion. 97i Had no effect on extracellular bacteria, did not affect cell viability and offered added value in combination with antibiotic treatment.

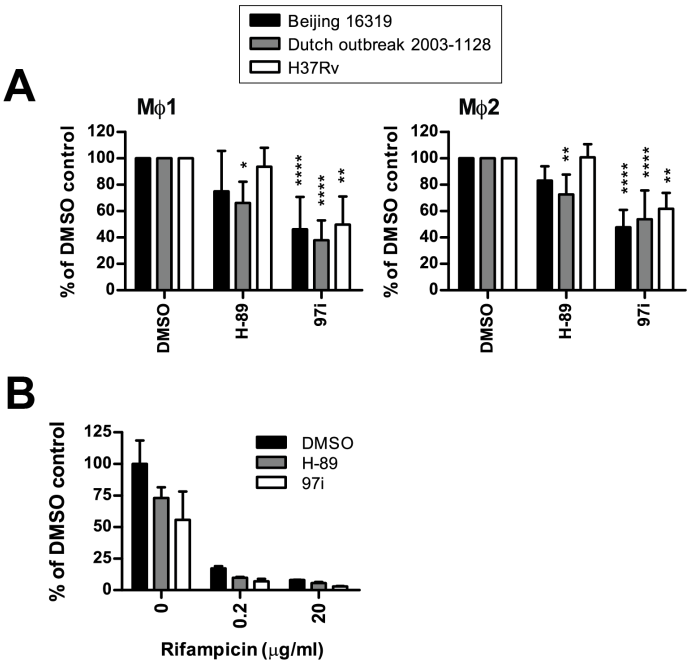

⬆ Figure 4. 97i efficacy testing in MDR-*Mtb* infections and in combination with antibiotics.

A. CFU assay of human type 1 and type 2 Mϕs infected with *Mtb* Beijing strain 16319, Dutch outbreak *Mtb* strain 2003-1128 or H37Rv, and treated with 10 μM H-89 or 97i or DMSO at equal v/v. Bars depict pooled results from macrophages from at least 3 individual donors, expressed as a percentage of the DMSO control. Statistical significance was tested using a two-way ANOVA with Dunnett multiple test correction. **B.** CFU assay of MelJuSo cells infected with *Mtb* and treated with a combination of rifampicin and 10 μM of either H-89 or 97i. Rifampicin was used at a concentration within the range of patient serum concentrations (20 μg/ml)[39], or at a suboptimal concentration (0.2 μg/ml). Data are expressed as a percentage of the DMSO control not treated with rifampicin.
(* = p-value <0.05, ** = p-value <0.01, *** = p-value <0.001, **** = p-value <0.0001).

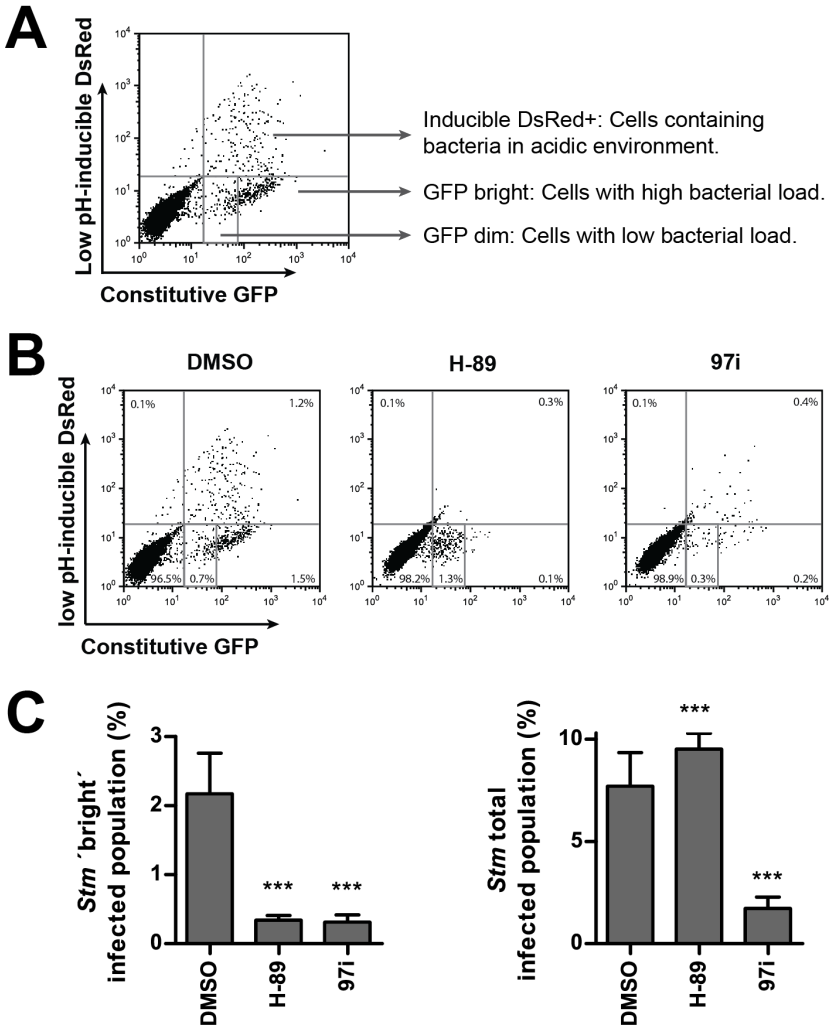

⬆ Figure 5. Analysis of *Stm* intracellular trafficking upon 97i treatment.

A. Example dot-plot from flow cytometric analysis of HeLa cells infected with dual-reporter (constitutive GFP and low pH-inducible DsRed) *Stm*. Interpretation of the different fluorescent cell populations is indicated. **B.** Flow cytometry dot-plots of HeLa cells infected with dual-reporter *Stm* treated with 10 μM H-89 or 97i or DMSO at equal v/v are displayed as in **A**. **C.** Quantification of different fluorescent populations in HeLa cells infected with dual-reporter *Stm* treated with 10 μM H-89 or 97i or DMSO at equal v/v. The percentage of GFP 'bright' cells is displayed in the left panel, while the right panel shows the total percentage of GFP positive cells. Data are the mean ± standard deviation of 20 replicates. A representative experiment out of at least 3 experiments is shown. Statistical significance was tested using one-way ANOVA.
(*** = p-value <0.001).

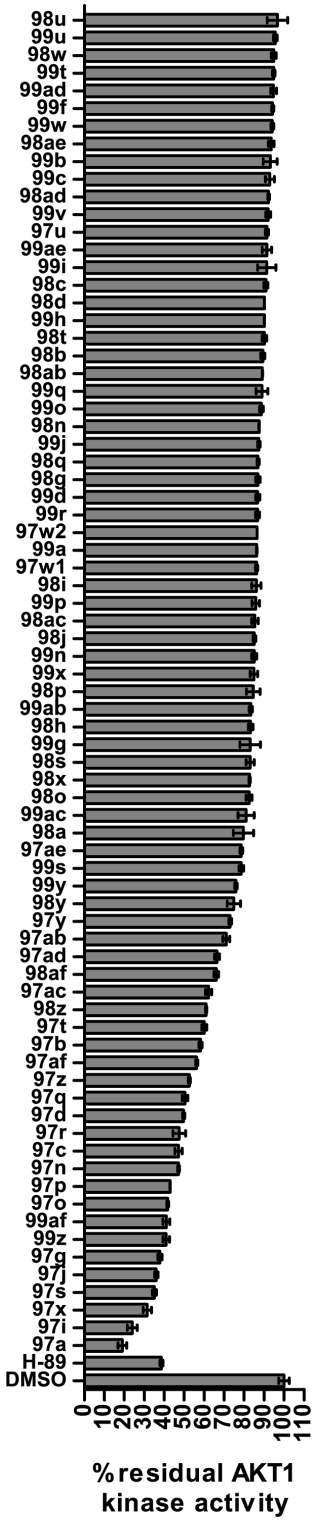

⬅ Figure 6. Analysis of *in vitro* AKT1 inhibition by the H-89 analogue compound library.
In vitro AKT1 inhibition assay using the compound library of H-89 analogues. Graph shows the percentage of residual AKT1 activity in the presence of chemical compounds at a 1.7 μM concentration (previously determined as an optimal concentration for AKT1 inhibition by H-89 *in vitro*[17]) compared to DMSO at equal v/v. Data are expressed as a percentage of the DMSO control value ± standard deviation.

Analysis of intracellular trafficking of *Stm* upon 97i treatment.

To gain insight into the possible mechanism of action of 97i, particularly its impact upon bacterial trafficking to different intracellular compartments, we employed a HeLa infection model using a dual-reporter *Stm.* This *Stm* strain constitutively expresses GFP and is capable of low pH-inducible expression of destabilized DsRed to visualize *Stm* trafficking to non-acidic (GFP+/DsRed-) as well as acidic (GFP+/DsRed+) compartments. Using this model, cells containing high or low bacterial loads can also be clearly distinguished based on fluorescence intensity (**Figure 5A**), as previously reported[34]. H-89 treatment resulted in clearance of all *Stm* from acidic compartments, while a dim GFP signal still remained present (**Figure 5B**). Quantification of these data demonstrated that despite equal inhibition of *Stm* proliferation by both H-89 and 97i (**Figure 5C, left panel**), the total GFP positive cell population did not decrease upon H-89 treatment (**Figure 5C, right panel**). This indicated that either non-proliferating bacteria, dead (but intact) bacteria or free GFP remained intracellularly after H-89 treatment. In contrast, 97i almost completely abrogated fluorescent signals from the cells (**Figure 5B** and **Figure 5C, right panel**), indicating induction of a mechanism resulting in degradation of all *Stm*-associated proteins.

In summary, 97i reduced a population of *Stm*-infected cells that is not sensitive to H-89, indicating that 97i induces a different inhibitory mechanism than H-89.

Structure-activity relationship analysis confirms molecularly that *Mtb* survival is regulated by host kinases other than AKT1.

To study the role of AKT1 inhibition in the intracellular bacterial inhibition exerted by our novel compounds, an *in vitro* AKT1 kinase inhibition screen was performed for all synthesized compounds (**Figure 6**) and cross-referenced with the *Stm* and *Mtb* inhibition screening data from **Figure 3A** (**Figure 7A**). In the AKT1 inhibition screen, 97i was identified as a strong AKT1 inhibitor. However, a group of compounds that strongly inhibited intracellular *Mtb* without affecting AKT1 activity was also identified (**Figure 7A, right panel**), suggesting that inhibition of other kinases might contribute to *Mtb* inhibition. Stratification of the *Stm* 'bright' screening data by AKT1 inhibitory activity (using the median AKT1 inhibition of the whole dataset as a cut-off) revealed that compounds exerting strong AKT1 inhibition were significantly stronger inhibitors of *Stm* (**Figure 7B, left panel**), confirming our previous findings[17]. An identical analysis of the *Mtb* screening data revealed no difference in *Mtb* inhibition by either weak or strong AKT1 inhibitors. Despite this lack of correlation between AKT1 inhibition and the *Mtb* bacterial

➡ Figure 7 (next page). Comparison of *in vitro* AKT1 inhibition and intracellular bacterial inhibition by the H-89 analogue compound library.
A. AKT1 inhibition *in vitro* was compared to the *Stm* 'bright' (left panel), *Stm* total (middle panel) and *Mtb* (right panel) compound screening data (**Figure 3A**). The percentage of residual kinase activity is plotted on the y-axis against the effect of compound treatment on the bacterial load (expressed as a z-score) on the x-axis for each compound. Each data point represents an individual compound. H-89 is indicated in black and 97i is shown as an open circle. A group of weak AKT1 inhibitors that decreased *Mtb* intracellular survival is indicated by a dashed box (short dashes). Dashed line (long dashes): hit cut-off from *Stm* and *Mtb* compound screens (see legend **Figure 3A**). **B.** *Stm* 'bright' (left panel), *Stm* total (middle panel) and *Mtb* (right panel) compound screening data (from **Figure 3A**) expressed as a z-score and stratified using a cut-off at the median AKT1 inhibition of the whole dataset. Data points represent individual compounds. H-89 is indicated in black and 97i is shown as an open circle. Statistical significance was tested using a Mann-Whitney test. **C.** Relationship between chemical structure and AKT1 inhibitory activity for compounds carrying a residue at the R_1, R_2 or R_3 positions. Residual AKT1 activity *in vitro* is plotted for individual compounds. An open circle indicates 97i. Dashed line: level of AKT1 inhibition by H-89. Statistical significance was tested using a one-way ANOVA with Bonferroni multiple comparison test. **D.** Structure-activity relationship for compounds carrying a residue at the R_1, R_2 or R_3 positions against bacterial infection loads, comparing the *Stm* 'bright' (left panel), *Stm* total (middle panel) and *Mtb* (right panel) compound screening data (from **Figure 3A**). An open circle indicates 97i. Dashed line: bacterial load upon H-89 treatment. Statistical significance was tested using a one-way ANOVA with Bonferroni multiple comparison test.
(* = p-value <0.05, ** = p-value <0.01, *** = p-value <0.001).

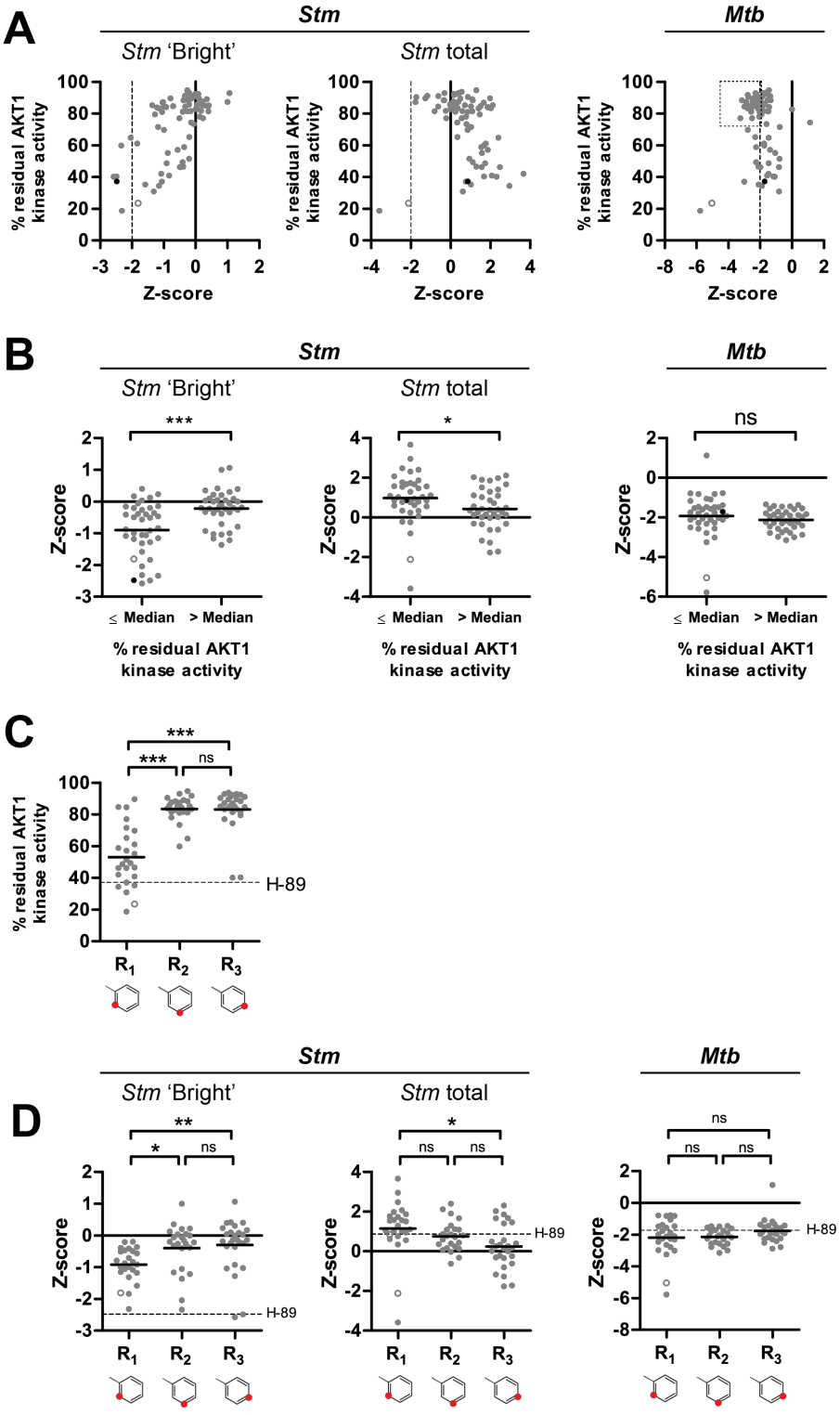
A
Stm
Mtb
Stm 'Bright'
Stm total
% residual AKT1 kinase activity
Z-score
B
***
*
ns
≤ Median
> Median
% residual AKT1 kinase activity
C
***
***
ns
H-89
R1
R2
R3
D
**
*
ns
*
ns
ns
ns
ns
ns
H-89
R1
R2
R3

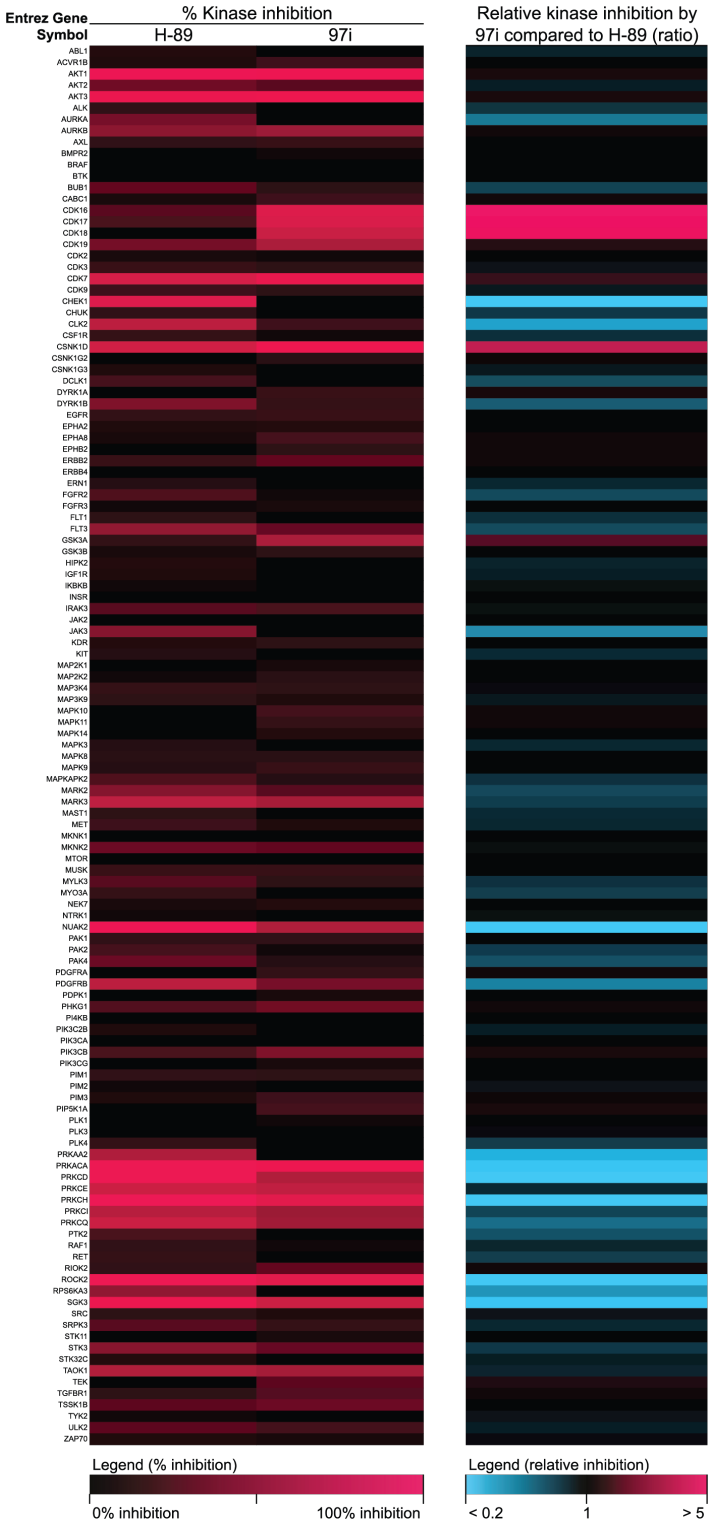

← Figure 8. Kinase inhibition profiles of compounds H-89 and 97i. Heat maps displaying *in vitro* kinase inhibition by compounds H-89 and 97i. The left panel shows the actual percentage of kinase inhibition by the compounds for the indicated kinases. The right panel shows the relative kinase inhibition of 97i compared to H-89 expressed as a ratio.

load, 97i strongly decreased both the total *Stm* infected and *Mtb* infected populations, indicating that kinases other than AKT1 may be involved in inhibiting intracellular *Mtb* (**Figure 7B, right panel**) and decreasing the total *Stm*-infected population (**Figure 7B, middle panel**).

Next, we studied whether the chemical conformation of the inhibitors (**Figure 2**) was associated with their AKT1 inhibitory activity. Compounds carrying any residue at the R_1 position were significantly better AKT1 inhibitors than compounds carrying residues at R_2 or R_3 positions (**Figure 7C**). This structure-activity relationship resulted in functional consequences as compounds carrying a residue at R_1 inhibited *Stm* intracellular survival significantly better than the R_2 or R_3 variants when analyzing the *Stm* 'bright' population (**Figure 7D, left panel**). Again, no difference was observed between compound groups for *Mtb* intracellular survival (**Figure 7D, right panel**). In contrast, 97i (a compound from the R_1 group) strongly decreased the *Stm* total and *Mtb* infected populations, further indicating that bacterial inhibition exerted by 97i is dependent on AKT1 and one or more additional kinase(s).

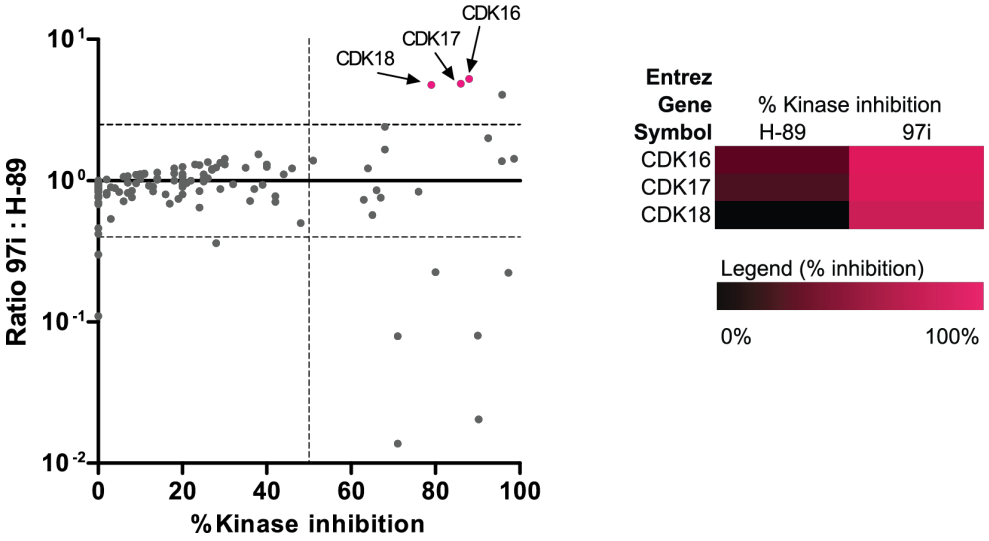

⬆ Figure 9. Identification of candidate target kinases of 97i.

A scatterplot displaying relative kinase inhibition by 97i compared to H-89 as a function of the percentage of kinase inhibition by 97i is displayed in the left panel. Each data point represents an individual kinase. Horizontal dashed lines indicate a 2.5-fold (higher or lower) difference in kinase inhibition compared to H-89. The vertical dashed line is a cut-off at 50% kinase inhibition. Data points in magenta represent the three kinases (CDK16, CDK17 and CDK18) that were not strongly inhibited by H-89 (< 50% inhibition), were inhibited by at least 50% by 97i and displayed at least a 2.5-fold enhanced inhibition by 97i compared to H-89. The right panel shows the percentage of kinase inhibition of CDK16, CDK17 and CDK18 by 97i and H-89 as a heat map as in **Figure 8**.

Taken together, these data strongly suggest a role for kinases other than AKT1 in regulation of *Mtb* intracellular survival, whereas in contrast AKT1 alone plays a dominant role in regulating *Stm* intracellular survival.

Identification of CDK18 as a target of 97i and as a putative host regulator of intracellular bacterial survival.

As 97i likely induced a different inhibitory mechanism than H-89, and both H-89 and 97i inhibit AKT1, we next set out to identify other kinases that are targeted by 97i but not by H-89. To this end we compared the *in vitro* kinome inhibitory capacity of H-89 and 97i by screening them against a panel of 123 kinases representing all major branches of the human protein kinase phylogeny (**Figure 8**). The results of this kinome scan revealed a high (but not complete) degree of similarity between the target profiles of 97i and H-89 and confirmed that both compounds similarly inhibited AKT1. To identify the kinases responsible for the enhanced bacterial inhibition by 97i compared to H-89, we focused on kinases that 1) were not strongly inhibited (< 50%) by H-89; 2) were inhibited significantly (≥ 50%) by 97i and 3) displayed at least a 2.5-fold increased inhibition by 97i compared to H-89. Kinases CDK16, CDK17 and CDK18 fulfilled these criteria and were therefore selected as targets of 97i (**Figure 9**). We next explored whether inhibition of CDK16, 17 or 18 by 97i is responsible for the enhanced reduction of bacterial load compared to H-89. Therefore, we employed siRNA to silence CDK16, 17 or 18 in the presence or absence of H-89 treatment (**Figure 10**). Indeed, a combination of H-89 treatment and CDK18 silencing mimicked the strong inhibitory effect of 97i in our HeLa-*Stm* infection model (**Figure 10**). No such effect was observed when silencing CDK16 or CDK17 either alone or in combination with H-89 treatment (data not shown).

In conclusion, we have identified CDK16, CDK17 and CDK18 as novel target kinases of 97i and demonstrated that targeting CDK18 in addition to kinases inhibited by H-89 exerts superior host-mediated *Stm* inhibition.

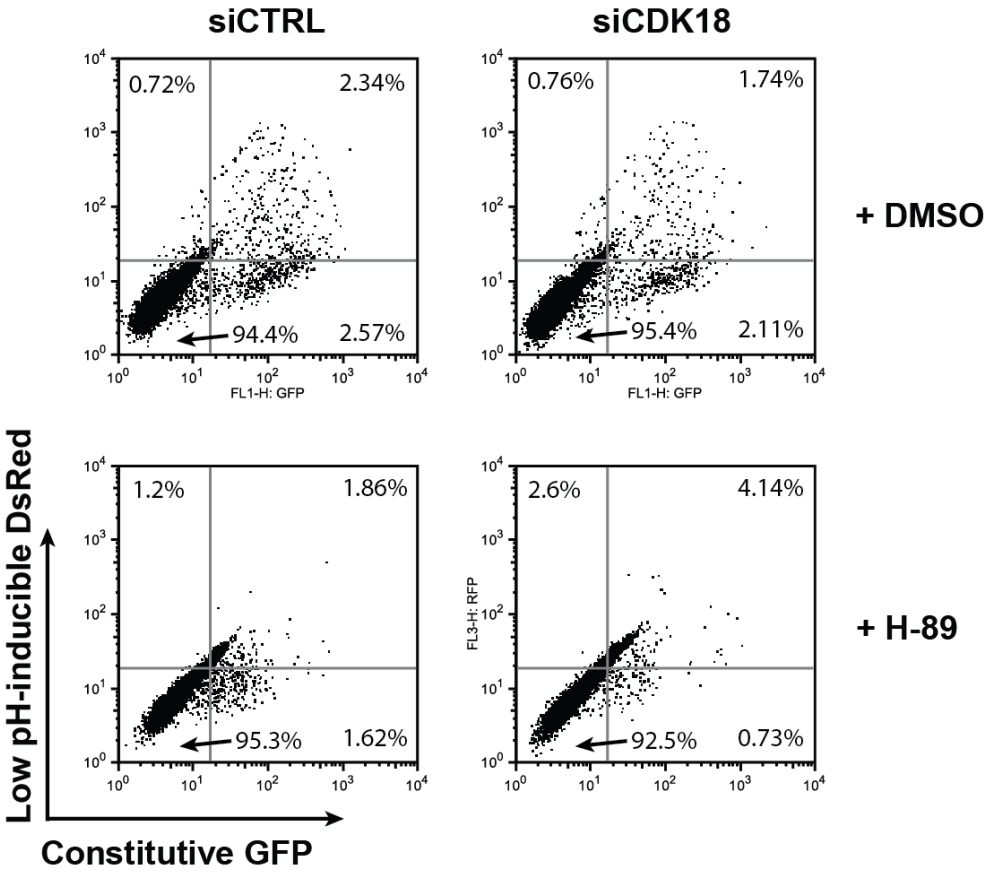

⬆ Figure 10. Confirmation of CDK18 as a regulator of intracellular bacterial survival.
Flow cytometry dot-plots of siRNA-silenced HeLa cells infected with dual-reporter *Stm* either treated with 10 μM H-89 or DMSO at equal v/v are displayed as in **Figure 5A**. CDK18 was silenced (siCDK18), while a scrambled siRNA pool (siCTRL) was used as a negative control.

Discussion

Here we report the chemical genetic identification of a novel host-directed kinase inhibitor, 97i, which targets the PCTAIRE-family kinase member CDK18 to enhance host control of *Stm* and possibly other major intracellular human pathogens, including *Mtb*, MDR-*Mtb* and other *Salmonella* species, in human cells. Greatly increased host-mediated *Mtb* inhibition was achieved by enhancing the chemical structure of H-89, modifying its target specificity to include CDK18, alongside kinases readily targeted by H-89. We previously demonstrated that H-89 is able to partially inhibit intracellular *Mtb,* indicating that pathways targeted by H-89,

including AKT1, are involved in *Mtb* control. Here we demonstrate that supplementation of H-89 treatment with genetic silencing of CDK18 mimicked the effect of 97i treatment in our HeLa-*Stm* infection model. These data suggest that the inability of H-89 to inhibit CDK18 might also be responsible for its inability to achieve significant *Mtb* inhibition.

The PCTAIRE kinases are a distinct family of cyclin-dependent kinases (CDKs) consisting of CDK16, CDK17 and CDK18 (PCTAIRE-1, PCTAIRE-2 and PCTAIRE-3, respectively) [40]. Despite being part of the CDK family, the role of PCTAIRE kinases in cell cycle regulation is still under debate and their cellular-molecular functions are poorly understood. However, several recent publications have begun to shed light on their cellular and molecular functions. In contrast to other CDKs, the PCTAIRE family of kinases can display a cytosolic localization. The PCTAIRE kinases CDK16 and CDK18 were previously shown to interact with COPII to modulate secretory cargo transport from the ER, indicating a role in vesicle transport. Interestingly, this process could be partly inhibited by H-89[41]. Here, we demonstrate that H-89 partly inhibits CDK16 and CDK17, but not CDK18. In contrast, 97i inhibits all three PCTAIRE family members. In our study we confirmed CDK18 as an important PCTAIRE kinase for control of intracellular bacterial infection. Further studies on HDT drugs will need to focus on identifying the contribution of individual PCTAIRE kinases in controlling of bacterial infection, and subsequently to improve inhibitor selectivity for the relevant kinases involved. In several recent studies in cancer, selective inhibitors of CDK16 were employed, providing a possible starting point for further chemical modifications and rational drug design[42,43]. In further support of a role for CDK18 in vesicle transport as well as a possible link between CDK18 and phagocytosis, Matsuda *et al*. recently reported that CDK18 is a negative regulator of the kinase FAK, which in turn regulates the RhoGTPases Rac1 and RhoA[44]. Rac1 and RhoA are central regulators of actin cytoskeleton reorganization[45], which is not only linked to cell motility and adhesion, but is also an essential mechanism driving phagocytosis and phagosome maturation[46]. Therefore, CDK18 might be directly involved in regulation of phagosome maturation, e.g. via FAK. Our own (unpublished) data agree with a role for FAK in the regulation of intracellular bacterial survival, as silencing of FAK increased the bacterial load of both *Stm* and *Mtb*.

Other potential functions of PCTAIRE kinases in intracellular bacterial infection might be related to immune modulation. Recently, CDK16 knockdown was shown to sensitize tumor cells to TNF-family cytokines[43]. Even though this may have not been a contributing factor in our infection models, 97i might exert an additional immunomodulatory effect *in vivo* by sensitizing infected macrophages to TNF-family cytokines through its inhibition of multiple PCTAIRE kinases. Further studies in more complex (*in vitro* and *in vivo*) model systems should be performed to confirm this potentially beneficial immunomodulatory effect of 97i. In another study focusing on inhibition of the IL-1β-induced inflammatory response by *Klebsiella pneumoniae* (*K. pneumoniae*), CDK18 was identified as one of the proteins required for this inhibition and this process was dependent on the epidermal growth factor receptor (EGFR) [47]. This suggests another potential immunomodulatory role for CDK18 in *Mtb* infection, as IL-1β was previously demonstrated to balance type I interferon production towards a

protective phenotype during *Mtb* infection[27]. As we previously also identified growth factor receptor tyrosine kinase signaling (including via EGFR) as a central host regulatory pathway controlling *Mtb* infection[34], similar inhibitory mechanisms might be employed by both *K. pneumoniae* and *Mtb*.

Though not extensively studied, CDK18 was previously linked to *Stm* infection and may be one of the host targets actively manipulated by the bacterium. Bioinformatics analysis of phosphoproteomics data of *Stm*-infected cells identified CDK18 as a possible upstream regulator involved in phosphorylation events in infected cells induced by *Stm* infection[48]. Even though CDK18 was not selected as a top candidate in the study by Rogers *et al.*, our own data show that CDK18 may indeed be mechanistically involved in *Stm* infection outcome.

Our chemical genetic approach emphasizes the complexity of interactions between *Mtb* and the host. The demonstration that inhibition of multiple kinases is essential for *Mtb* control points to a potential limitation of single gene based RNAi approaches since identification of kinase interactions and interaction networks is not feasible in a single-knockdown setting. Therefore, the chemical lead optimization approach and subsequent target identification as we have followed here might be a powerful alternative for identifying novel drug targets for TB, by virtue of the fact that chemical compounds rarely have a single target.

Regardless of their mode of action, the novel inhibitors identified in our screens display promising effects in our infection models. First of all, the ability of these compounds to further reduce the *Mtb* bacterial load following *in vitro* rifampicin treatment provides proof-of-principle that host-directed compounds can be used to either induce further inhibition of bacteria that are less susceptible to antibiotics or to render them more susceptible to the microbicidal effects of antibiotics. If further developed, similar compounds might offer ways to shorten the unusually long (minimum 6 months) antibiotic course of TB treatment as well as decrease the probability of *de novo* antibiotic resistance by targeting the host rather than the bacterium[15,16]. Importantly, our novel kinase inhibitors are equally active against both a laboratory strain (H37Rv) as well as clinical (MDR) isolates. This provides an important proof-of-concept that host-directed compounds such as 97i can be applied to complement classical antibiotics for treatment of MDR bacterial infections.

In conclusion, we identified 97i as a novel host-directed kinase inhibitor, which controls major intracellular human pathogens, including *Mtb*, MDR-*Mtb* and *Salmonella* species in human cells. We further demonstrated that 97i inhibited intracellular *Stm* by not only targeting AKT1 but also the PCTAIRE-family kinase member CDK18. Further work is required to confirm whether these kinases are also involved in controlling intracellular *Mtb*. The potent new chemical inhibitor 97i may be used as a basis for next-generation host-directed therapeutics against intracellular bacterial infections.

Materials & Methods

Synthesis of the kinase inhibitor library

Synthesis of the compound library is described in "Synthetic studies on kinase inhibitors and cyclic peptides: strategies towards new antibiotics", Adriaan W. Tuin, 2008 (https://openaccess.leidenuniv.nl/bitstream/handle/1887/13365/Proefschrift+AW_Tuin+alles.pdf?sequence=7).

Reagents

H-89 dihydrochloride, Rifampicin and Kanamycin were purchased from Sigma-Aldrich, Zwijndrecht, The Netherlands. Ampicillin was acquired from Calbiochem Merck-Millipore, Darmstadt, Germany. Hygromycin B was supplied by Life Technologies-Invitrogen, Bleiswijk, The Netherlands.

Cell culture

Cell culture was performed as previously described[34]. In short, HeLa and MelJuSo cell lines were maintained at 37°C and 5% CO_2 in Gibco Iscove's Modified Dulbecco's Medium (IMDM, Life Technologies-Invitrogen) supplemented with 10% fetal bovine serum (FBS, Greiner Bio-One, Alphen a/d Rijn, The Netherlands), 100 units/ml Penicillin and 100 µg/ml Streptomycin (Life Technologies). Type 1 and type 2 Mϕs were generated by differentiating monocytes of healthy donors for 6 days with 5 ng/ml recombinant granulocyte macrophage-colony stimulating factor (GM-CSF, BioSource Life Technologies-Invitrogen) or 50 ng/ml recombinant macrophage-colony stimulating factor (M-CSF, R&D Systems, Abingdon, United Kingdom) respectively, as previously reported[49]. Mϕs were maintained in Gibco Roswell Park Memorial Institute (RPMI) 1640 medium (Life Technologies-Invitrogen) supplemented with 10% FBS and 2 mM L-Alanyl-L-Glutamine (PAA, Linz, Austria).

Bacterial culture

Bacterial strains used are displayed in **Table 1**. Mycobacteria were cultured in Difco Middlebrook 7H9 broth (Becton Dickinson, Breda, The Netherlands) supplemented with 10% ADC (Becton Dickinson), 0.5% Tween-80 (Sigma-Aldrich) and appropriate antibiotics. *Stm* was cultured on Difco Luria-Bertani (LB) agar (Becton Dickinson) or in Difco LB broth (Becton Dickinson) supplemented with appropriate antibiotics.

Stm and *Mtb* infections

Stm and *Mtb* infections were performed as previously described[34]. In short, 10,000 HeLa or MelJuSo cells seeded in 96-well flat-bottom plates were inoculated with 100 µl of the bacterial suspension at MOI 10 (unless otherwise indicated), centrifuged for 3 minutes at 800 rpm and incubated at 37°C/5% CO_2 for 20 minutes if infected with *Stm* or 60 minutes if infected with *Mtb*. Plates were then washed with culture medium containing 30 µg/ml gentamicin sulfate (Lonza BioWhittaker, Basel, Switzerland) and incubated at 37°C and 5% CO_2 in medium containing 5 µg/ml gentamicin and indicated chemical compoundsat 10 µM

Table 1. Bacterial strains, plasmids used for fluorescent protein expression and their respective antibiotic selection markers.

Base strain	Plasmid	Antibiotic resistance *(source, concentration)*
Mtb H37Rv.	pSMT3[Phsp60/DsRed].	Hygromycin *(plasmid, 50 µg/ml).*
Mtb H37Rv.	pSMT3[Phsp60/destabilized DsRed].	Hygromycin *(plasmid, 50 µg/ml).*
Mtb Beijing family China (Kremer 43) 16319.	None.	Rifampicin, Isoniazid, Ethambutol, Pyrazinamide *(intrinsic, n/a).*
Mtb Dutch outbreak 2003-1128.	None.	Rifampicin, Isoniazid, Streptomycin, Claritromycin *(intrinsic, n/a).*
Stm SL1344.	pMW211[C.10E/DsRed] (Constitutive promotor).	Ampicillin *(plasmid, 100 µg/ml).*
Stm SL1344.	pMW215[PpagC/DsRed] (Low-pH inducible promotor).	Ampicillin *(plasmid, 100 µg/ml).*
Stm SL1344.	pMW215[PpagC/DsRed] (Low pH-inducible promotor). pMW211[C.10E/GFP] (Constitutive promotor).	Ampicillin *(plasmid, 100 µg/ml).* Kanamycin *(plasmid, 100 µg/ml).*

concentration (unless indicated otherwise) until readout by flow cytometry or CFU, as indicated.

Chemical compound treatment

10,000 HeLa or MelJuSo cells or were seeded per well in 96-well flat-bottom plates or 300,000 primary Mϕs were plated in 24-well flat-bottom plates in appropriate culture medium without antibiotics one day prior to infection with *Mtb* or broth-grown *Stm.* Infected cells were treated overnight with chemical compounds at a 10 µM concentration (unless otherwise indicated) in medium containing 5 µg/ml gentamicin.

siRNA transfections

3,000 HeLa or MelJuSo cells were reverse-transfected with ON-TARGETplus siRNA pools (Thermo Fisher Dharmacon, Waltham Massachusetts, USA) at a 50 nM concentration using 0.2 µl Dharmafect1 (Thermo Fisher Dharmacon) per well in a flat-bottom 96-well plate in appropriate culture medium without antibiotics. Cells transfected with siRNA were infected with *Mtb* at MOI 1000 24 hours post transfection and incubated for an additional 48 hours and infections with agar-grown *Stm* were carried out at MOI 500 72 hours post transfection and incubated overnight, unless otherwise indicated.

Colony forming unit assay

CFU assays were performed using the track dilution method described previously[50]. In short, serial dilutions of bacterial suspensions and 10 µl drops were spotted on square agar plates (Becton Dickinson). The plates were then placed at an angle to allow the drops to spread out on the plates.

Bacterial growth assay

100 µl *Mtb* or *Stm* culture (OD_{600} of 0.1) was plated in a flat-bottom 96-well plate containing 100 µl of indicated chemical compounds at 20 µM in 7H9 broth for *Mtb* or LB broth for *Stm*. The plate was incubated at 37°C and absorbance was measured at a 550 nm wavelength at indicated time points on a Mithras LB 940 plate reader (Berthold Technologies, Bad Wildbad, Germany).

AKT1 kinase inhibition assay

AKT1 kinase inhibition assays were performed as previously reported[17]. Compounds were tested at 1,7 µM concentration in the presence of 100 µM ATP.

Kinase inhibitor profiling

Kinase inhibitor target profiling was performed commercially at 10 µM using the ScanEDGE panel for the KINOMEscan platform (DiscoveRx, Fremont California, USA).

Statistics

Student's T-test (two groups, normally distributed), Mann-Whitney test (two groups, non-parametric), one-way ANOVA with Dunnett's multiple comparison test (multiple groups) and two-way ANOVA with Bonferroni post test (multiple comparisons, grouped data) were performed using GraphPad Prism version 7.0 for Mac OS X (GraphPad Software, San Diego California USA, www.graphpad.com). Screening statistics were performed as previously reported[34], according to guidelines from the NIH Chemical Genomics Center[38]. Z-scores were calculated by dividing the difference between the percentage of gated fluorescent events (bacterial load) of each screening replicate and the average percentage of fluorescent events of the DMSO control by the DMSO control's standard deviation. For the primary compound screen data, z-scores were calculated using the same formula, but the average percentage of fluorescent events and the standard deviation of all samples on each plate (instead of the DMSO control) was used to provide plate normalization. Subsequently, the average DMSO z-score was subtracted from each sample.

Acknowledgements

This project was funded by the European Union's Seventh Programme for research, technological development and demonstration under grant agreement N° PhagoSys HEALTH-F4-2008-223451; NEWTBVAC HEALTH.F3.2009 241745, TANDEM project Grant Agreement N° 305279. We also gratefully acknowledge the support of the Netherlands Organization for Health Research and Development

(ZonMw-TOP grant 91214038) and Technology Foundation STW (grant 13259). The funders had no role in study design, data collection and analysis, decision to publish, or preparation of the manuscript.

We thank Dick van Soolingen and Kirsten Kremer (RIVM, Bilthoven, the Netherlands) for providing the MDR-*Mtb* strains.

References

1. Ottenhoff, T. H. M. The knowns and unknowns of the immunopathogenesis of tuberculosis. *Int. J. Tuberc. Lung Dis.* **16,** 1424–1432 (2012).
2. World Health Organization. *Global Tuberculosis Report 2017*. 1–249 (2017).
3. Ottenhoff, T. H. M. Overcoming the global crisis: 'yes, we can', but also for TB ... ? *Eur. J. Immunol.* **39,** 2014–2020 (2009).
4. Jassal, M. S. & Bishai, W. R. Epidemiology and challenges to the elimination of global tuberculosis. *CLIN INFECT DIS* **50 Suppl 3,** S156–64 (2010).
5. Ottenhoff, T. H. M. New pathways of protective and pathological host defense to mycobacteria. *Trends Microbiol.* **20,** 419–428 (2012).
6. Smith, S. I., Seriki, A. & Ajayi, A. Typhoidal and non-typhoidal Salmonella infections in Africa. *Eur. J. Clin. Microbiol. Infect. Dis.* **35,** 1913–1922 (2016).
7. Barry, C. E. & Blanchard, J. S. The chemical biology of new drugs in the development for tuberculosis. *Curr Opin Chem Biol* **14,** 456–466 (2010).
8. Norrby, S. R., Nord, C. E., Finch, R.European Society of Clinical Microbiology and Infectious Diseases. Lack of development of new antimicrobial drugs: a potential serious threat to public health. *Lancet Infect Dis* **5,** 115–119 (2005).
9. Becker, D. *et al.* Robust Salmonella metabolism limits possibilities for new antimicrobials. **440,** 303–307 (2006).
10. Makarov, V. *et al.* Benzothiazinones kill Mycobacterium tuberculosis by blocking arabinan synthesis. *Science* **324,** 801–804 (2009).
11. Christophe, T. *et al.* High content screening identifies decaprenyl-phosphoribose 2' epimerase as a target for intracellular antimycobacterial inhibitors. *PLoS Pathog* **5,** e1000645 (2009).
12. Willand, N. *et al.* Synthetic EthR inhibitors boost antituberculous activity of ethionamide. *Nat. Med.* **15,** 537–544 (2009).
13. Lawn, S. D. & Zumla, A. I. Tuberculosis. *Lancet* **378,** 57–72 (2011).
14. O'Neill, J. *Tackling drug-resistant infections globally: final report and recommendations*. (London: Wellcome Trust & HM Government, 2016).
15. Guler, R. & Brombacher, F. Host-directed drug therapy for tuberculosis. *Nature Chemical Biology* **11,** 748–751 (2015).
16. Hawn, T. R., Shah, J. A. & Kalman, D. New tricks for old dogs: countering antibiotic resistance in tuberculosis with host-directed therapeutics. *Immunol. Rev.* **264,** 344–362 (2015).
17. Kuijl, C. *et al.* Intracellular bacterial growth is controlled by a kinase network around PKB/AKT1. **450,** 725–730 (2007).
18. Kumar, D. *et al.* Genome-wide analysis of the host intracellular network that regulates survival of Mycobacterium tuberculosis. *Cell* **140,** 731–743 (2010).
19. Jayaswal, S. *et al.* Identification of host-dependent survival factors for intracellular Mycobacterium tuberculosis through an siRNA screen. *PLoS Pathog* **6,** e1000839 (2010).

20. Sundaramurthy, V. *et al.* Integration of chemical and RNAi multiparametric profiles identifies triggers of intracellular mycobacterial killing. *Cell Host and Microbe* **13,** 129–142 (2013).
21. Machado, D. *et al.* Ion Channel Blockers as Antimicrobial Agents, Efflux Inhibitors, and Enhancers of Macrophage Killing Activity against Drug Resistant Mycobacterium tuberculosis. *PLoS ONE* **11,** e0149326 (2016).
22. Napier, R. J. *et al.* Imatinib-sensitive tyrosine kinases regulate mycobacterial pathogenesis and represent therapeutic targets against tuberculosis. *Cell Host and Microbe* **10,** 475–485 (2011).
23. Subbian, S. *et al.* Phosphodiesterase-4 inhibition alters gene expression and improves isoniazid-mediated clearance of Mycobacterium tuberculosis in rabbit lungs. *PLoS Pathog* **7,** e1002262 (2011).
24. Subbian, S. *et al.* Phosphodiesterase-4 inhibition combined with isoniazid treatment of rabbits with pulmonary tuberculosis reduces macrophage activation and lung pathology. *Am. J. Pathol.* **179,** 289–301 (2011).
25. Koo, M.-S. *et al.* Phosphodiesterase 4 inhibition reduces innate immunity and improves isoniazid clearance of Mycobacterium tuberculosis in the lungs of infected mice. *PLoS ONE* **6,** e17091 (2011).
26. Vilaplana, C. *et al.* Ibuprofen therapy resulted in significantly decreased tissue bacillary loads and increased survival in a new murine experimental model of active tuberculosis. *Journal of Infectious Diseases* **208,** 199–202 (2013).
27. Mayer-Barber, K. D. *et al.* Host-directed therapy of tuberculosis based on interleukin-1 and type I interferon crosstalk. **511,** 99–103 (2014).
28. Datta, M. *et al.* Anti-vascular endothelial growth factor treatment normalizes tuberculosis granuloma vasculature and improves small molecule delivery. *Proc Natl Acad Sci USA* **112,** 1827–1832 (2015).
29. Oehlers, S. H. *et al.* Interception of host angiogenic signalling limits mycobacterial growth. **517,** 612–615 (2015).
30. Schiebler, M. *et al.* Functional drug screening reveals anticonvulsants as enhancers of mTOR-independent autophagic killing of Mycobacterium tuberculosis through inositol depletion. *EMBO Molecular Medicine* **7,** 127–139 (2015).
31. Skerry, C. *et al.* Simvastatin increases the in vivo activity of the first-line tuberculosis regimen. *J. Antimicrob. Chemother.* **69,** 2453–2457 (2014).
32. Stanley, S. A. *et al.* Identification of host-targeted small molecules that restrict intracellular Mycobacterium tuberculosis growth. *PLoS Pathog* **10,** e1003946 (2014).
33. Li, Q. *et al.* Novel high throughput pooled shRNA screening identifies NQO1 as a potential drug target for host directed therapy for tuberculosis. *Sci Rep* **6,** 27566 (2016).
34. Korbee, K. J. *et al.* Combined chemical genetics and data-driven bioinformatics approach identifies receptor tyrosine kinase inhibitors as host-directed antimicrobials. *Nat Commun* **9,** 358 (2018).
35. Vergne, I., Chua, J., Singh, S. B. & Deretic, V. Cell biology of mycobacterium tuberculosis phagosome. *Annu. Rev. Cell Dev. Biol.* **20,** 367–394 (2004).

36. Brumell, J. H. & Grinstein, S. Salmonella redirects phagosomal maturation. *Current Opinion in Microbiology* **7,** 78–84 (2004).
37. Sogi, K. M., Lien, K. A., Johnson, J. R., Krogan, N. J. & Stanley, S. A. The Tyrosine Kinase Inhibitor Gefitinib Restricts Mycobacterium tuberculosis Growth through Increased Lysosomal Biogenesis and Modulation of Cytokine Signaling. *ACS Infect Dis* **3,** 564–574 (2017).
38. Singhal, A. *et al.* Metformin as adjunct antituberculosis therapy. *Science Translational Medicine* **6,** 263ra159–263ra159 (2014).
39. Peloquin, C. A. Using therapeutic drug monitoring to dose the antimycobacterial drugs. *Clin. Chest Med.* **18,** 79–87 (1997).
40. Mikolcevic, P., Rainer, J. & Geley, S. Orphan kinases turn eccentric: a new class of cyclin Y-activated, membrane-targeted CDKs. *Cell Cycle* **11,** 3758–3768 (2012).
41. Palmer, K. J., Konkel, J. E. & Stephens, D. J. PCTAIRE protein kinases interact directly with the COPII complex and modulate secretory cargo transport. *Journal of Cell Science* **118,** 3839–3847 (2005).
42. Dixon-Clarke, S. E. *et al.* Structure and inhibitor specificity of the PCTAIRE-family kinase CDK16. *Biochem. J.* **474,** 699–713 (2017).
43. Yanagi, T., Shi, R., Aza-Blanc, P., Reed, J. C. & Matsuzawa, S.-I. PCTAIRE1-knockdown sensitizes cancer cells to TNF family cytokines. *PLoS ONE* **10,** e0119404 (2015).
44. Matsuda, S., Kawamoto, K., Miyamoto, K., Tsuji, A. & Yuasa, K. PCTK3/CDK18 regulates cell migration and adhesion by negatively modulating FAK activity. *Sci Rep* **7,** 45545 (2017).
45. Groves, E., Dart, A. E., Covarelli, V. & Caron, E. Molecular mechanisms of phagocytic uptake in mammalian cells. *Cell. Mol. Life Sci.* **65,** 1957–1976 (2008).
46. Kinchen, J. M. & Ravichandran, K. S. Phagosome maturation: going through the acid test. *Nat Rev Mol Cell Biol* **9,** 781–795 (2008).
47. Frank, C. G. *et al.* Klebsiella pneumoniae targets an EGF receptor-dependent pathway to subvert inflammation. *Cellular Microbiology* **15,** 1212–1233 (2013).
48. Rogers, L. D., Brown, N. F., Fang, Y., Pelech, S. & Foster, L. J. Phosphoproteomic analysis of Salmonella-infected cells identifies key kinase regulators and SopB-dependent host phosphorylation events. *Science Signaling* **4,** rs9 (2011).
49. Verreck, F. A. W., de Boer, T., Langenberg, D. M. L., van der Zanden, L. & Ottenhoff, T. H. M. Phenotypic and functional profiling of human proinflammatory type-1 and anti-inflammatory type-2 macrophages in response to microbial antigens and IFN-gamma- and CD40L-mediated costimulation. *Journal of Leukocyte Biology* **79,** 285–293 (2006).
50. Jett, B. D., Hatter, K. L., Huycke, M. M. & Gilmore, M. S. Simplified agar plate method for quantifying viable bacteria. *BioTechniques* **23,** 648–650 (1997).